JOURNAL OF GEOPHYSICAL RESEARCH, VOL. 114, A00C13, doi:10.1029/2008JA013583, 2009

Timing and localization of near-Earth tail and ionospheric signatures during a substorm onset

C. Gabrielse,[1] V. Angelopoulos,[1] A. Runov,[1] H. U. Frey,[2] J. McFadden,[2] D. E. Larson,[2] K.-H. Glassmeier,[3] S. Mende,[2] C. T. Russell,[1] S. Apatenkov,[4] K. R. Murphy,[5] and I. J. Rae[5]

Received 19 June 2008; revised 6 October 2008; accepted 27 October 2008; published 31 January 2009.

[1] On 16 February 2008, the THEMIS spacecraft (probes) bracketed the near-Earth signatures of a substorm onset as identified in the THEMIS ground-based observatories measuring an AE_{TH} index up to 180 nT. The main onset was associated with the formation and tailward release of a plasmoid (a proto-plasmoid) at $X_{GSM} = -18.3\ R_E$ and a dipolarization in the inner part of the plasma sheet at $X_{GSM} = -11.0\ R_E$. The time history and geometry of the event in the tail are consistent with magnetic reconnection as the cause of the substorm expansion onset process. Two activations of the plasma sheet, evidenced by tailward streaming of energetic ions and southward or bipolar signatures of the magnetic field, preceded the main substorm. The first activation was associated with an intensification of a high-latitude arc, while the second was associated with the onset of ULF pulsations at midlatitude and low-latitude stations. We conclude that near-Earth plasma sheet activity that may also be due to reconnection and may be related to nonsubstorm arc intensifications can precede substorm onset by several minutes. In particular, high-latitude arcs do not appear to result in substorm initiation even though they may occur in close temporal and spatial proximity to the substorm arc.

Citation: Gabrielse, C., et al. (2009), Timing and localization of near-Earth tail and ionospheric signatures during a substorm onset, *J. Geophys. Res.*, *114*, A00C13, doi:10.1029/2008JA013583.

1. Introduction

[2] Substorms, originally defined by *Akasofu* [1964], are now known to be the result of solar wind energy transferred to the Earth's magnetosphere when interplanetary magnetic field (IMF) lines become connected to Earth's magnetic field lines when the IMF is pointing southward. Energy is stored in the tail until a sudden release, resulting in particle heating and kinetic energy, global reconfigurations of the magnetosphere, and several space and ground observed phenomena. Because these phenomena are initially confined in space but quickly expand away from their initial location both in space and on the ground [*Ohtani and Kokubun*, 1991; *Sergeev et al.*, 1996a; *Angelopoulos et al.*, 1997], it is necessary to have several spacecraft aligned down the tail, parallel to the Sun-Earth line along with continent-scale images of the aurora and ionospheric currents, in order to determine the causal relationship of the events which lead to substorm onset. Two main magnetospheric processes have been suggested as the initiation of substorm onset: current disruption, a near-Earth dipolarization process around 10 R_E, or magnetic reconnection around 20–30 R_E [*Lui*, 1996; *Baker et al.*, 1996]. Since simultaneous satellite-to-satellite and space-ground correlations were previously obtained by serendipity, and thus were not optimal, the exact location of the substorm initialization in space has remained unanswered. Specifically, azimuthal and down-tail propagation effects and lack of simultaneous observations at the regions in which these phenomena start has rendered even state-of-the-art timing indefinite [*Sergeev et al.*, 1995; *Liou et al.*, 2002; *Kepko et al.*, 2004; *Lui et al.*, 2007].

[3] The THEMIS mission [*Angelopoulos*, 2008] was designed to provide optimized spacecraft (probe) conjunctions in order to determine the correct onset trigger. Five identical satellites (probes), designed to line up periodically along the X_{gsm} direction and measure in situ the plasma sheet particles and fields at ~10 R_E and at ~20–30 R_E downtail. Major alignments (with all 5 satellites) occur every 4 days, while minor alignments (involving 3–4 out of the five satellites) occur on the second day after a major alignment.

[4] Alignments take place over the North American sector, which is instrumented with a network of ground-based observatories (GBOs) [*Mende et al.*, 2007, 2008], equipped with white light All Sky Imagers (ASIs) [*Harris et al.*, 2008] and ground magnetometers [*Russell et al.*, 2009] to determine the meridian and time of substorm onset to

[1]IGPP, ESS, University of California, Los Angeles, California, USA.
[2]Space Sciences Laboratory, University of California, Berkeley, California, USA.
[3]Technische Universität Braunschweig, Braunschweig, Germany.
[4]University of St. Petersburg, St. Petersburg, Russia.
[5]Department of Physics, University of Alberta, Edmonton, Alberta, Canada.

0148-0227/09/2008JA013583$09.00

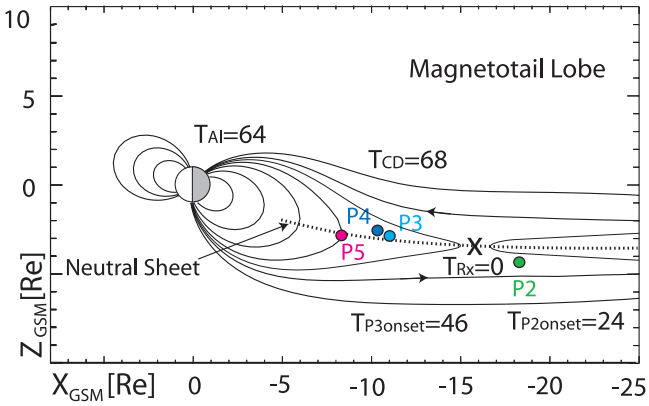

Satellite	Color	X	Y	Z	Neutral Sheet
THEMIS-A (P5)		-8.313	-1.003	-2.824	-0.2
THEMIS-B (P1)		-18.724	11.549	-3.872	-3.7
THEMIS-C (P2)		-18.283	3.357	-4.328	-1.5
THEMIS-D (P3)		-11.015	2.377	-2.772	0
THEMIS-E (P4)		-10.337	3.187	-2.544	0.1

Figure 1. Projections of the THEMIS probes in the $X-Z_{GSM}$ plane along with representative field lines and neutral sheet location in geocentric solar magnetospheric (GSM) coordinates. The table is in units of R_E, where the probe distance from the neutral sheet is given in the neutral sheet column. TH-B (P1) is red, TH-C (P2) is green, TH-D (P3) is cyan, TH-E (P4) is dark blue, and TH-A (P5) is magenta.

within 3 s. In this paper we present timing results from THEMIS for an isolated substorm which occurred on 16 February 2008. We show that magnetic reconnection was initiated prior to the onset of ground auroral intensification and poleward expansion, and that the substorm event was preceded by plasma sheet activations, also likely due to reconnection, with corresponding auroral activations that were distinct from and were not causally related to the major substorm onset. One of the two plasma sheet activations was related to a high-latitude arc, protruding over a GBO adjacent to the station where the substorm arc was observed. The high-latitude arc began as a faint but stable background East–West arc, which then intensified as a whole as well as dynamically intensified and dimmed over time. This temporal brightening indicates preexisting activity in the plasma sheet, resembling poleward boundary intensifications (PBIs) as described by *Zesta et al.* [2006]. Our observations suggest that magnetotail reconnection proceeds as a series of distinct bursts over several minutes prior to onset and on occasion related to arcs, but that the activation leading up to the main onset is more intense and possibly more global, resulting in the main substorm onset.

[5] Figure 1 is a pictorial representation of where the four THEMIS probes in the minor conjunction were located in space projected in the $X-Z_{GSM}$ plane relative to the Earth's magnetic field lines. The times on Figure 1 are a summary of our results and will be discussed within this paper. The T96 model [*Tsyganenko*, 1995] was used to project the probe locations along magnetic field lines to the ionosphere. The probe foot points, plotted along with THEMIS ground observatories are shown in Figure 2. The circles represent each ground-based observatory's all-sky imager field of view. Probes TH-C (P2), TH-D (P3) and TH-E (P4) map approximately within the field of view of Sanikiluaq (SNKQ). Mapping uncertainties from different Tsyganenko models are expected to be of the order of one hour of magnetic local time, and further mapping improvements for this event can be obtained by either MHD modeling of the field aligned currents [e.g., *Angelopoulos et al.*, 2008; J. Raeder et al., Open GGCM simulations for the THEMIS mission, submitted to *Space Science Reviews*, 2008] or from careful modification of the Tsyganenko model parameters to match the THEMIS probe observations (M. Kubushkina et al., Toward adapted time-dependent magnetospheric models: A simple approach based on tuning the standard model, manuscript in preparation, 2008).

2. Ground-Based Observations

[6] Midlatitude data from the intermagnet network were used in Figure 3 to fit model parameters of the ring current disturbance (DR) and the substorm current wedge (SCW) to determine their magnitudes and locations as a function of time [*Horning et al.*, 1974; *Sergeev et al.*, 1996a]. This models currents as infinitely thin wires and fits observed magnetic variations within 5–10%. Probes TH-C (P2), TH-D (P3) and TH-E (P4) lie within the SCW sector (see Figure 3c) approximately within one hour of local time from the center of the substorm current wedge. These results provide some confidence that the phenomena observed at the time on the above probes are related to the modeled substorm activity.

[7] Figure 4 shows an overview of the ground observations for this event. A sudden increase in the THEMIS AE index, AE_{TH}, to 180 nT was observed around 0451:35 UT, indicating the expansion phase onset of an isolated substorm. Timing was established on the basis of the inflection point of the index. Note that AE_{TH} was constructed from all the THEMIS stations available at the time, including those shown in Figure 2 and (although quiet day subtraction has not been implemented) it has potentially higher sensitivity to

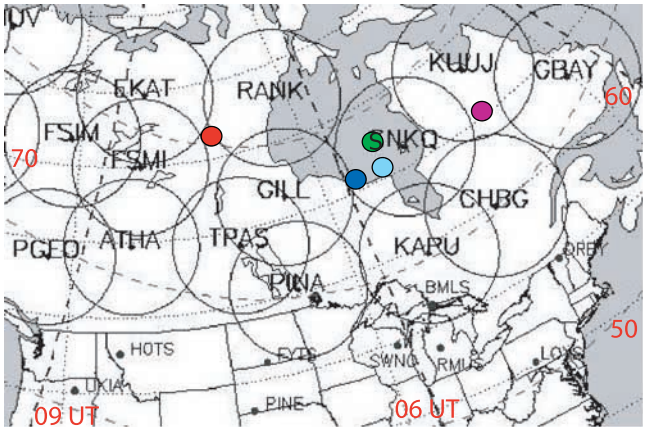

Figure 2. THEMIS probe foot points and THEMIS ground stations. P1 is red, P2 is green, P3 is cyan, P4 is dark blue, and P5 is magenta. Dashed lines are corrected geomagnetic longitude (one per three hours of magnetic local time) and latitude (one per ten degrees) lines, whereas dotted lines are geographic longitude (one per three hours of geographic local time) and latitudes (one per five degrees).

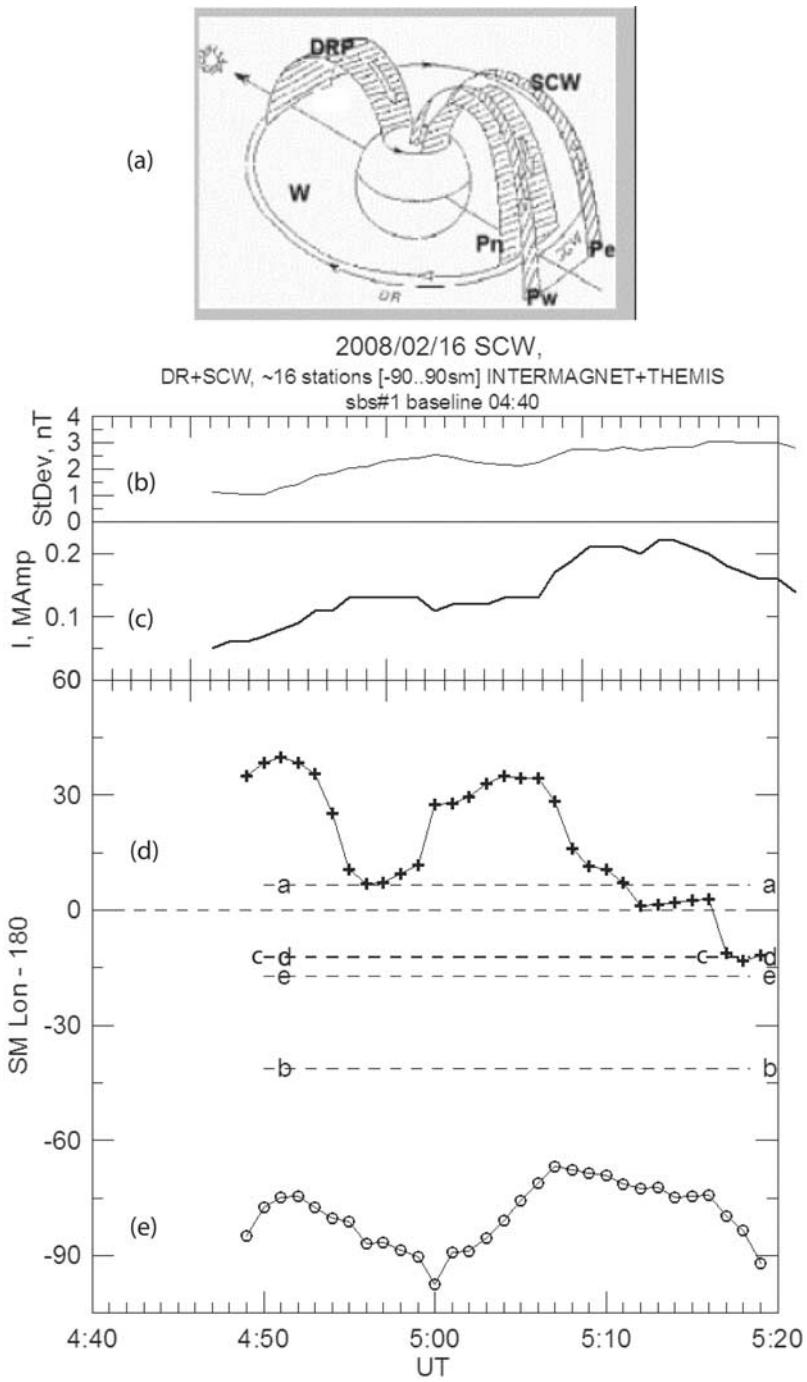

Figure 3. Modeling midlatitude ground magnetometer signatures to determine the central meridian, width, and intensity of near-Earth space currents. (a) Pictorial representation of the model used (composed of line currents or series of line currents). (b) Modeled intensity (MA) and longitude (degrees) of the current system components as a function of time past 0440 UT, specifically, (c) standard deviation of the observations versus model disturbances, (d) SCW current intensity in megaAmps, and (e) longitude of downward (crosses) and upward (circles) field aligned currents, in SM-180 coordinates (i.e., solar magnetospheric longitude minus 180°). Probe foot point locations are marked by the dashed lines.

localized auroral intensifications, pseudobreakups and small substorms than the traditional AE index [*Mayaud*, 1980].

[8] Determination of the time of single time of onset is not possible with the timing resolution capability afforded by THEMIS GBOs since different substorm onset indicators result in different onset times. Rather, in this paper we differentiate between the different classical substorm onset indicators and tabulate their onsets in time sequence, as they correspond to unique processes. The inflection point of the THEMIS AE index was tabulated, along with the other

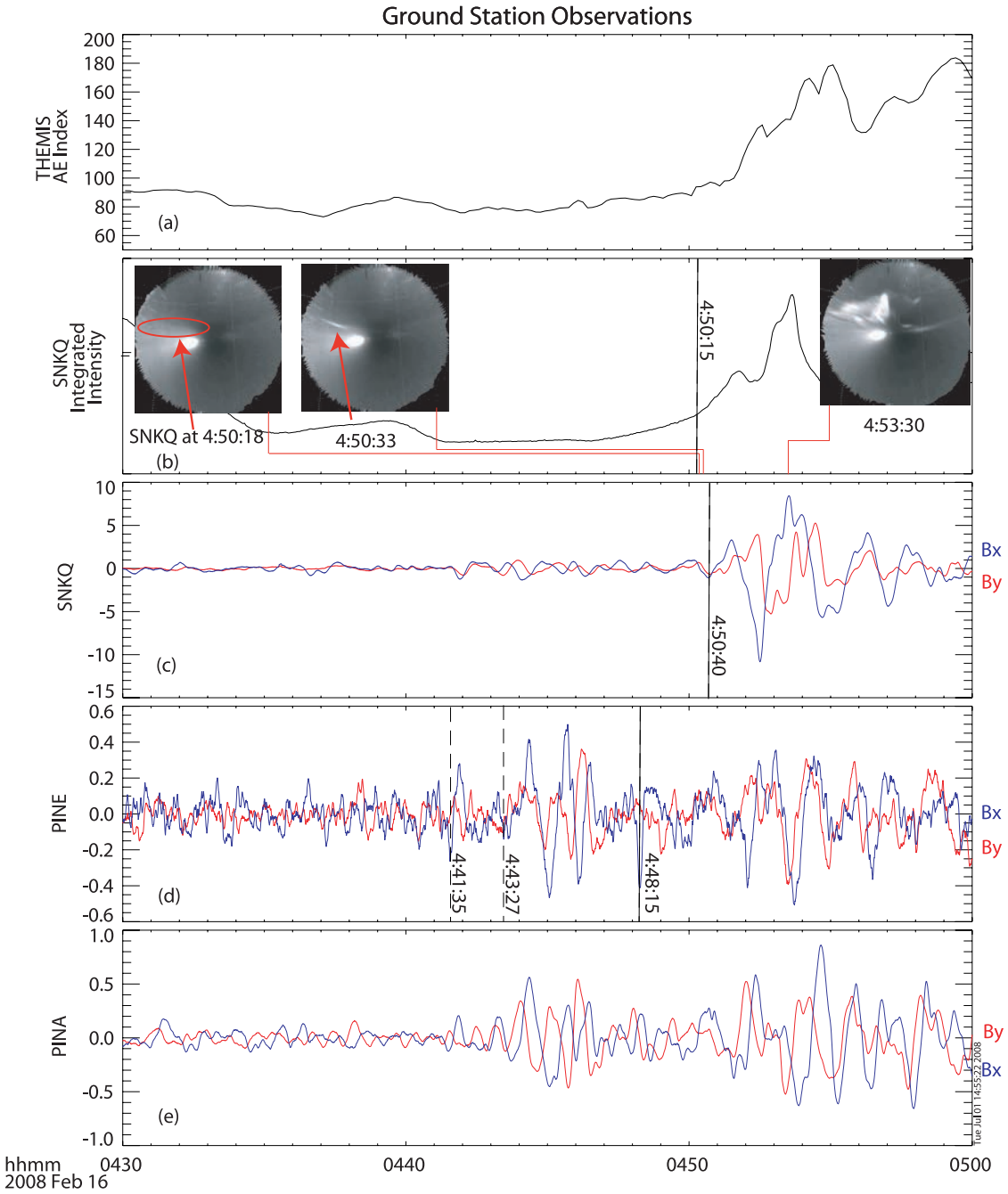

Figure 4. An overview plot from THEMIS ground observations. (a) AE index. (b) All-sky-imager data from SNKQ. The red arrow points to the first sign of auroral brightening at 0450:21. The ASI snapshot at 0450:33 shows the evolution of the brightening arm, and the 0453:30 snapshot shows the full aurora. The bright spot is the Moon. The plot is the integrated intensity (sum of AD units). (c–e) Pi2 waves as measured at SNKQ, PINE, and PINA. The solid line at 0450:15 represents the time that the slope in the integrated intensity increases. The dashed lines correlate to signatures in the Pi2s. The first one at 0443:30 marks the start of precursory Pi2s due to activity seen at the high-latitude station RANK. The dashed line at 0448:15 marks a local Pi2 burst at PINE, while the dashed line at 0450:40 marks the onset of Pi2 waves (above the background waves) at SNKQ.

timing observables, in Table 1 (see section 4), but was not used further as an indication of timing of substorm or ionospheric processes because of the limitations arising from background removal (the index is treated predominantly as a quick-look proxy of activity and near-real time event detection).

[9] Global (continent-wide) mosaics for this event indicate activity at stations Rankin Inlet (RANK) and Sanikiluaq (SNKQ). All-sky-imager cadence is 3 s, and is synchronized to the same UT second between all imagers in the array. The first sign of auroral intensification related

to the aforementioned AE_{TH} increase was observed about a minute prior to the AE_{TH} rise, at the all-sky-imager at SNKQ. Figure 4b shows the integrated intensity of the luminosity at SNKQ, in analog-to-digital (AD) units (a relative measure of the analog output of the measurement). The integrated intensity is more reliable in determining the onset of auroral brightening at that location than the images alone. Figure 4b also contains raw images from SNKQ, from select times. Note that in the images, top is north and right is east, as if looking at the aurora from space, and the bright spot is the Moon. On the basis of the inflection point of the luminosity we determined that rapid auroral brightening occurred at 0450:15 UT. Examination of the raw images shows that the onset occurred at 68° magnetic latitude. The weak auroral emission is circled in the image insert corresponding to the first perceptible auroral intensification in the ASIs. The all-sky-imager snapshot from 0450:33 is included also, in order to demonstrate the evolution of the aurora as the arc brightened but before it expanded poleward across the field of view. From these images it is evident that the aurora was intensifying but was stable, prior to 0450:39 UT. At 0450:42 UT the aurora started to exhibit poleward motion. At 0451:30 the ASI at RANK starts to see the substorm arc at the bottom of its FOV. By 0453:30 UT the aurora had expanded poleward, coincident with the peak of the integrated intensity as observed by the all-sky-imager at SNKQ, reaching a magnetic latitude of ~70.4°. (Faint traces of the westward traveling aurora are seen further north at RANK around 0457:40, not shown, but available in Animation S1.)[1] The times of rapid auroral intensification and poleward expansion are demarcated in Figure 4b and tabulated in Table 1.

[10] Additionally, we demarcate the onset of rapid substorm-related auroral intensification with a solid vertical line at 0450:15 UT and carry that as our marker of substorm activity in Figures 8 and 9. The poleward expansion, which happened 23 s later, may be a better definition of classical substorm expansion phase onset, since poleward expansion is a necessary part of the definition of classical substorms, whereas substorms which do not expand poleward are traditionally termed pseudobreakups [*Rostoker et al.*, 1980]. However, as we seek the first indication of rapid (explosive) energy release in the ionosphere to correlate with similar substorm signatures in space, and since the rapid auroral intensification preceded the poleward expansion, we use 0450:15 UT as our time of substorm activity onset on the ground.

[11] While a gradual intensification of the aurora did start earlier than 0450:15 UT, as evidenced by the linear increase in luminosity in Figure 4b, it is unclear (without further image processing) when and where exactly this slow intensification commenced on the west side of SNKQ, because of the dominance of the contamination from the moonlight and the presence of thin clouds. Station Gillam, to the West of SNKQ, was also covered by thin clouds in the presence of the Moon. Therefore although it is clear that no intense auroral brightening was observed at Gillam (and hence not discussed any further in this paper), that station also suffers from similar issues as SNKQ recognizing low-intensity auroral brightenings. There are documented cases where a fading of the onset occurs before the intensification [*Starkov et al.*, 2006], which is another reason why we chose the inflection point at 0450:15. At this time we can be sure that the intensification is not due to background lighting or subject to auroral fading before the beginning of the substorm active phase. For better identification of other activations in addition to the main onset, we now turn our attention to ground magnetometers.

[12] Figures 4c, 4d, and 4e show the Pi2 waves measured at SNKQ, (where the auroral onset was observed), Pine Ridge (PINE), a midlatitude station near the onset meridian, and Pinawa (PINA), a subauroral station also near the onset meridian.

[13] The auroral Pi2 waves associated with the abrupt intensification of the aurora were seen to start at 0450:40 UT, and marked by a dashed line in Figure 4c, determined as the beginning of the rise of a wave with increased signal amplitude above background. We used a boxcar filter with band pass in the range 10–120 s, to ensure good time resolution in the Pi2 band (40–120 s period) without filter distortions in the time domain. Figure 5a is a wavelet analysis of the transverse component of the ULF wave activity observed at SNKQ for six frequency bands (for details, see *Milling et al.* [2008] and *Murphy et al.* [2008]). This is an estimate of the spectrographic amplitude of the data in Figure 4c. Intensification of wavelet power in the Pi2 band (48–192 s, j = 6 band) at 0450:28 UT ± 32 s is evident. Power in both the Pi1 and Pi1/2 bands (6–96 s period; j = 7–9 in Figure 4) is observed to intensify at 0452:03 UT ± 32 s, ~2 min subsequent to the intensification of Pi2 power in the 48–196 s period wavelet band.

[14] The main onset, which was evident as Pi2 wave power increase in Figures 4c–4e at all stations at around 0450:40 UT, was preceded by wave power increases at several stations. Since it is known than midlatitude stations provide a global monitor of auroral activity [e.g., *Kepko et al.*, 2004] we chose station PINE to determine substorm precursor activation onsets. Three instances of Pi2 wave power intensification were evident in PINE and are demarcated with dashed lines in Figure 4d.

[15] The dashed line at 0448:15 UT marks a localized Pi2 wave burst measured at stations PINE and PINA, which occurred near the start of the gradual intensification of the aurora at SNKQ (Figure 4b) and the start of Pi2 power at station Gillam (not shown). ULF power enhancements are expected during the slow intensification phase of auroral arcs, prior to substorm expansion onset [e.g., *Rae et al.*, 2009; *Murphy et al.*, 2008]. We thus attribute this precursory Pi2 activity to the early intensification of the onset arc, though this cannot be proven owing to cloudiness. When we come to discuss our spacecraft observations, we can draw a correlation between this precursory Pi2 activity and small bipolar signatures, along with a slight tailward anisotropy.

[16] The dashed lines at 0441:35 and 0443:27 UT correspond to precursory Pi2 waves at PINE with counterparts at all nearby stations. It was also observed in the wavelet analysis of SNKQ data in Figure 5. These precursory Pi2 waves had no optical counterpart at low latitudes. However, a high-latitude activation or a preexisting high-latitude arc was captured at station Rankin Inlet (RANK). Figure 6 displays the evolution of the arc at RANK and the ensuing expansion of the classical substorm. The dynamics and

[1] Animation S1 is available in the HTML.

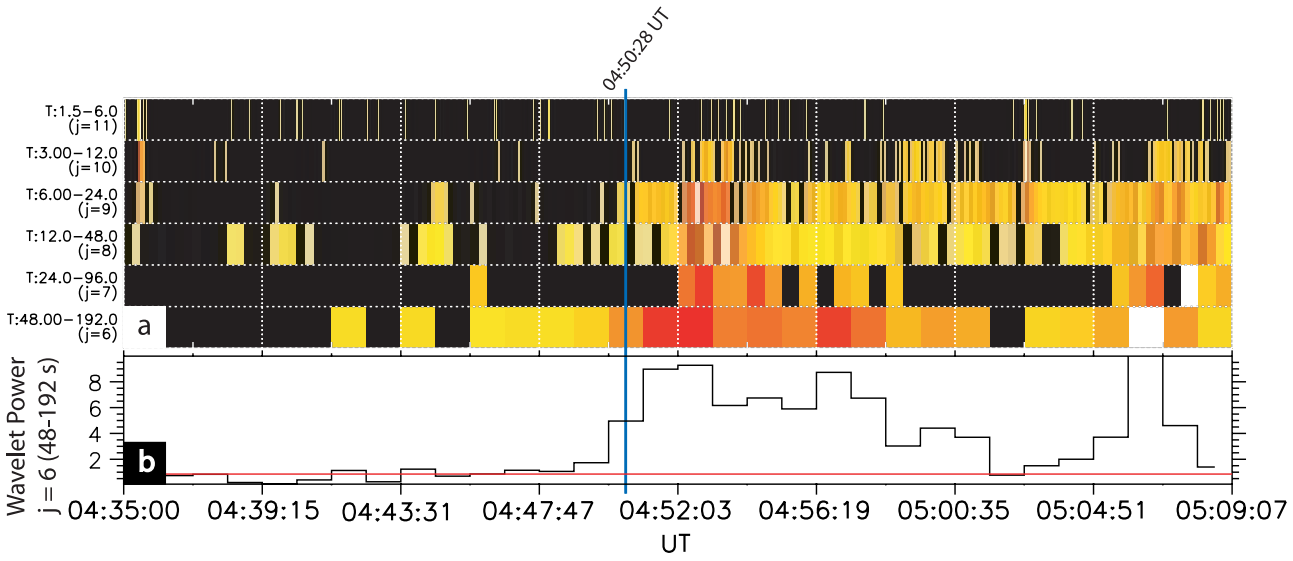

Figure 5. (a) Wavelet plot from SNKQ demonstrating ULF wave activity for six frequency bands. Color axis is the normalized color representation of the wavelet bands. It is at 0450:28 UT ± 32 s that we see the onset of Pi2 waves at SNKQ, in agreement with our visual determination of Pi2 power onset from Figure 4. (b) Time series of wavelet power in the 48–192 s j = 6 wavelet band. The red line is a ULF power threshold based upon a quiet time period, which we subtract from the color wavelet plot.

temporal brightening of the high-latitude arc can be more readily seen in Animation S1.

[17] It is evident that the high-latitude arc was present at 0430 UT, intensified at 0441 UT and again at 0443 UT. The two intensifications correlate well with the observations of the Pi2 waves at PINE.

[18] It is apparent that the kinked protrusion of the high-latitude arc did not reach the latitude of the arc that brightened at the ensuing substorm. As the expanding substorm arc started to evolve the high-latitude arc remained in place. The high-latitude arc was eventually engulfed by the activity of the new substorm arc as it was expanding poleward (by 0456 UT, not shown).

3. Observations in Space

[19] During the 16 February event, the THEMIS probes were in a minor conjunction. Four of the five probes, namely P2 ($X_{GSM} = -18.3$ R_E), P3 ($X_{GSM} = -11.0$ R_E), P4 ($X_{GSM} = -10.3$ R_E), were closely aligned along the Sun-Earth line as can be seen in Figures 1 and 2, while P1 ($X_{GSM} = -18.7$ R_E) was about 8.2 R_E duskward of P2, and P5 ($X_{GSM} = -8.3$) was −3.3 R_E dawnward of P3. Figure 7 is an overview plot of the three probes closest to the substorm meridian (P2, P3 and P4) including the magnetic field and the omnidirectional ion and electron energy-time spectrograms. (For information on the fluxgate magnetometer and the electrostatic analyzer, please refer to *Auster et al.* [2008] and *McFadden et al.* [2008], respectively.) The horizontal white line in the ion spectra plots is an energy gap between the maximum energy level measured by the ESA instrument and the minimum energy level measured by the SST instrument. Specifically we focus our attention on the interval around 0440–0500 UT. It is evident that all probes exhibited ion heating and magnetic field fluctuations during that time. Specifically, P2 observed a southward turning of the magnetic field, whereas the other two probes observed a reduction of Bx and an increase of northward Bz (dipolarization). These are classical signatures of reconnection observed by two spacecraft on either side of the reconnection side. The southward turning of Bz corresponds with the ULF pulsations observed at the midlatitude and low-latitude stations (PINE and PINA) in Figure 4.

[20] Because we are interested in the earliest signatures of onset in space at the meridian of the onset, and because P3 observed signatures of dipolarization earlier than P4, we focus our detailed analysis on P2 and P3 (see Figures 8 and 9, respectively).

[21] As seen in Figures 8a and 8b, P2 observed tailward flows, which peaked in magnitude at 0452:30 UT, near the

Figure 6. A timeline of all-sky-imager snapshots taken at RANK (top left) and SNKQ (bottom right). (a) High-latitude arc growth and development. Two minute cadence. (b) High-latitude arc growth and development. See some brightening corresponding to the 0441:35 Pi2 intensification at SNKQ. Thirty second cadence. (c) Thirty second cadence. See more intense light at 0443:00–0444:30. (Precursory Pi2 waves were measured at 0443:27.) (d) Sixty second cadence. (e) Three second cadence. At 0450:15 is substorm onset determined by integrated-intensity plot. Substorm onset visible at 0450:18 with first sign of auroral brightening, circled in red. (f) Six second cadence. Shows development of auroral arc (g) 30-s cadence. Auroral arc extends eastward and westward. See first signs of substorm-induced aurora at RANK. (h) Evolution into peak auroral activity and substorm dissipation over both stations.

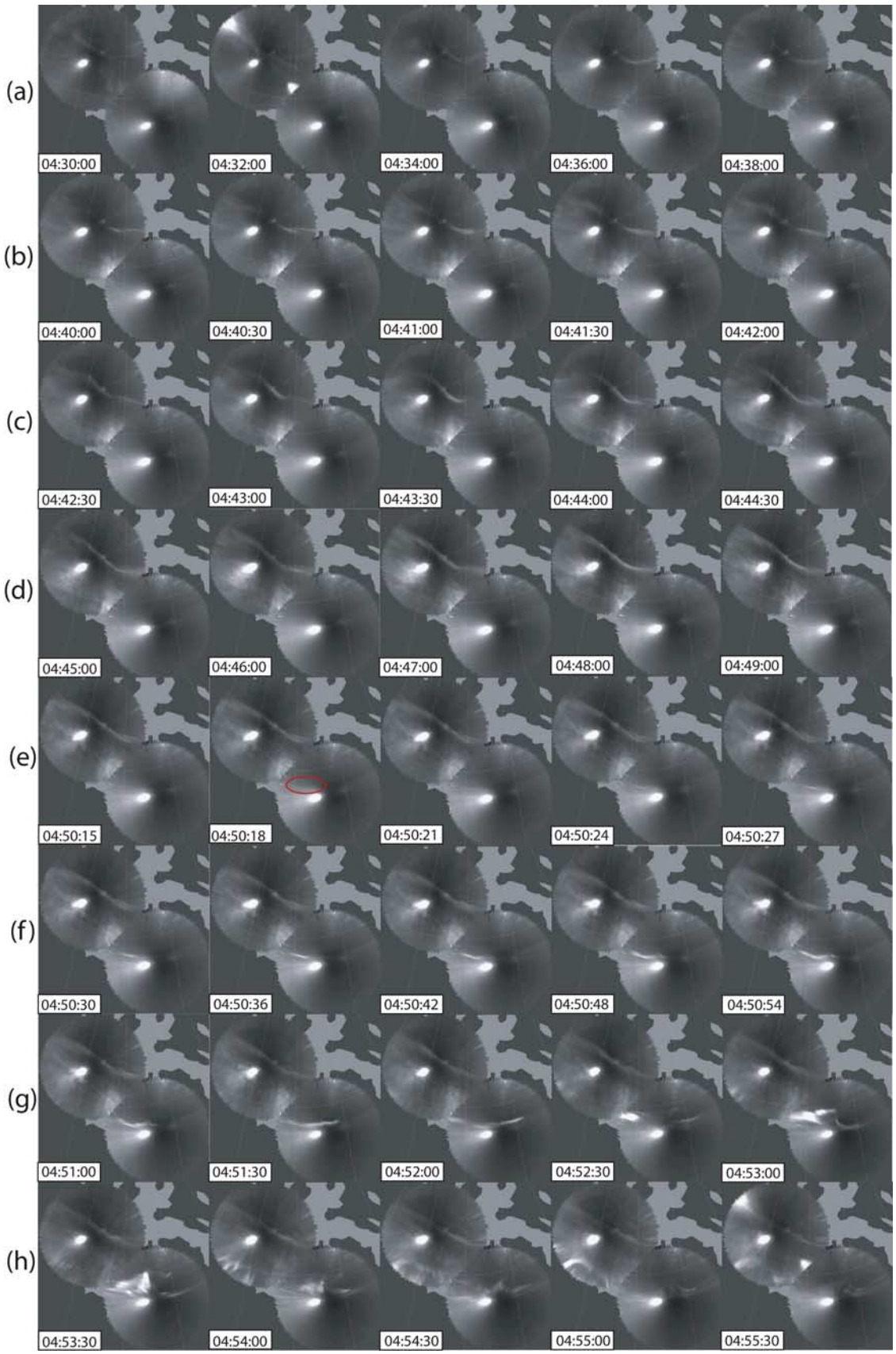
(a)
04:30:00
04:32:00
04:34:00
04:36:00
04:38:00
(b)
04:40:00
04:40:30
04:41:00
04:41:30
04:42:00
(c)
04:42:30
04:43:00
04:43:30
04:44:00
04:44:30
(d)
04:45:00
04:46:00
04:47:00
04:48:00
04:49:00
(e)
04:50:15
04:50:18
04:50:21
04:50:24
04:50:27
(f)
04:50:30
04:50:36
04:50:42
04:50:48
04:50:54
(g)
04:51:00
04:51:30
04:52:00
04:52:30
04:53:00
(h)
04:53:30
04:54:00
04:54:30
04:55:00
04:55:30

Figure 6

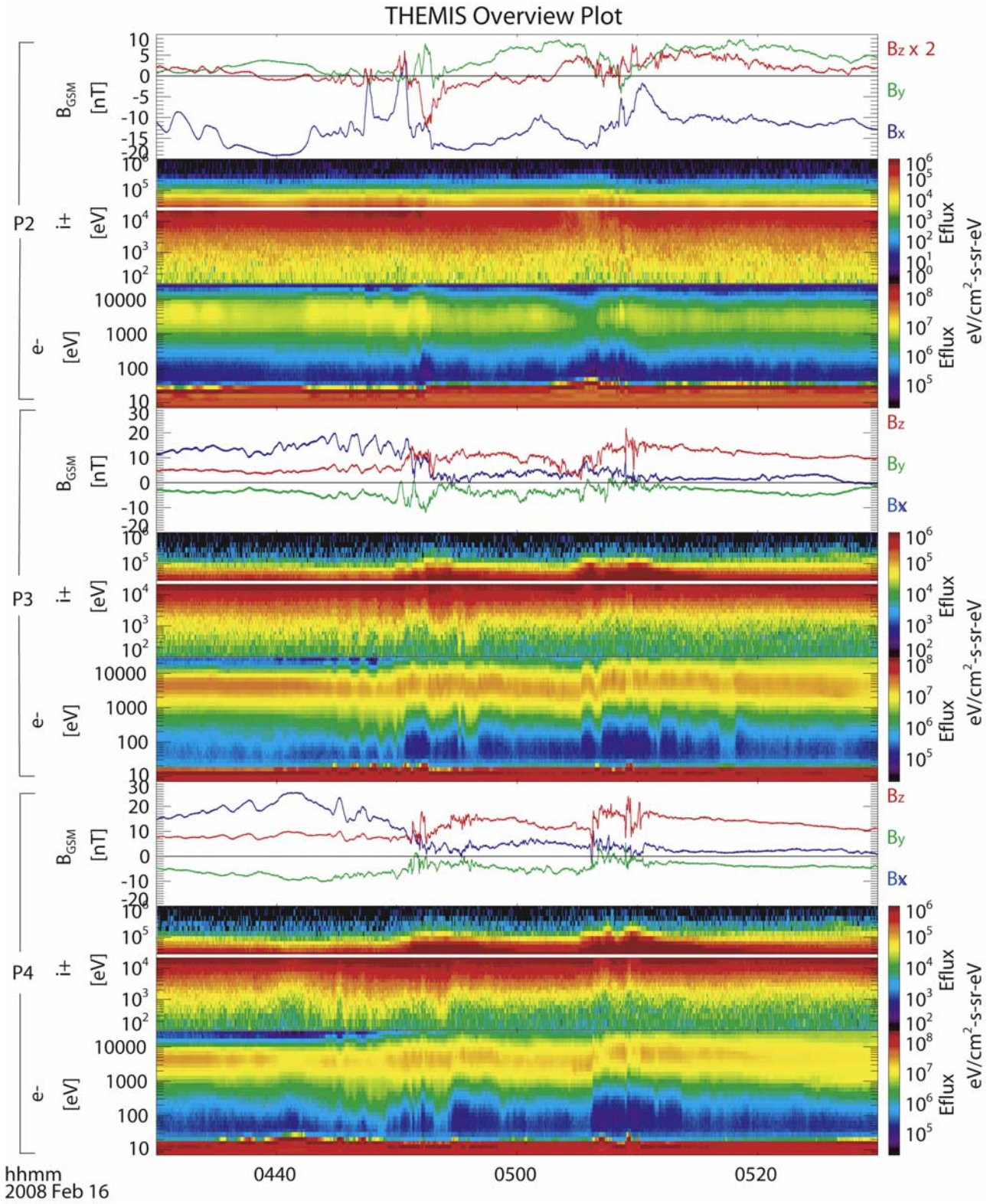

Figure 7. Overview of magnetic field and particle data for one hour at three second resolution, around the 0450:15 UT substorm. There are three panels per probe, measured by P2, P3, and P4, respectively. The three panels demonstrate the following: the magnetic field in GSM coordinates measured by the FGM instrument; ion energy spectra; and electron energy spectra. The latter two are the data combined from both ESA and SST instruments. All energy spectrograms show omnidirectional differential energy flux (efflux) in units of eV/(cm^2/s/str/eV). Note that in the first panel measured by P2, the Z component of the magnetic field, is multiplied by two in order to enhance its features for the reader.

time of the peak in the southward magnetic field. Around the same time, as seen in Figures 9a and 9b, P3 observed earthward flows near the time of a dipolarization at that location.

[22] The fast tailward flows on P2 were preceded by an interval of fluctuating (earthward – tailward) flows of smaller magnitude ($|Vx| < 50$ km/s). The dominant flow direction was duskward for 10 min prior to the event. Analysis of particle distributions indicates that the duskward flow is in good part due to the pressure gradient of the ions and thus consistent with a diamagnetic current across the tail. The intensification of the duskward flow is therefore an indication of the intensification of the cross tail current in the late growth phase of this substorm, and is evident in all probes outside of 10 R_E. We have also considered the anisotropy of energetic ions during this event. Figure 8f shows the angular anisotropy of near-equatorial particles of 25–50 keV. As described above the predominance of the duskward anisotropy is due to the north–south pressure gradient. The spectrogram is punctuated by intervals of enhanced flux, which corresponds to transient encounters with the near-neutral sheet plasma. Tailward anisotropies are seen close to the neutral sheet and are evaluated using the earthward to tailward flux ratio, normalized to the average, shown in Figure 8g. Tailward streaming (negative anisotropy) is enhanced several times during the interval prior to the fast tailward flows, including the time around 0450 UT, when the magnetic field was northward. These tailward streaming ions are evidence of particle acceleration which occurred earthward of P2, prior to the fast tailward flow of 0452 UT.

[23] Taking this tailward streaming into account, we interpret the bipolar signature in B_z as being due to a flux transfer event, or a plasmoid, that is slowly accelerating away from a near-Earth reconnection site. Spatial effects related to partial exit to the boundary layer also affect our observations: It is apparent that B_x, signifying distance to the neutral sheet, decreased to −15 nT at 0451 UT, which we interpret as a transient exit to the boundary due to plasma sheet flapping or thinning [*Baumjohann et al.*, 2007]. At that time, the flow velocity and the energetic particle anisotropy became earthward, which reflects mapping to a distant tail acceleration site. A minute later the fast tailward flow dominated again, as near-Earth reconnection is presumed to have reached sufficient strength to overcome the magnetic tension force from closed plasma sheet field lines. In that interpretation, it is apparent that the core of the plasmoid is not observed in situ, at 0451–0452 UT, because the plasmoid was confined initially to the neutral sheet, while P2 was at the outer layers of the plasma sheet. We suggest that on the trailing edge (after 0451:30 UT) fast flows are more intense because reconnection has had sufficient time to grow; and at that time the tailward flows are sent over a larger north–south extent of the plasma sheet because reconnection has detached a larger portion of the closed plasma sheet magnetic flux. Finally, Figure 8d shows the total pressure of plasma and magnetic field as well as the plasma pressure and magnetic pressure. Changes in the magnetic pressure are balanced by changes in the plasma pressure, resulting in a constant total pressure.

[24] The total pressure shows a peak near the time of the center of the bipolar signature in B_z, which is an expected behavior during the passage of a plasmoid core underneath a spacecraft. Thus, although the plasmoid core was not measured in situ, its passage was remotely sensed from the local peak in the plasma pressure.

[25] We refer to this plasmoid as a "proto-plasmoid" [*Ieda et al.*, 1998] because it was observed as it was being generated within the plasma sheet. We select the onset time of the plasmoid observation to be 0449:35 UT, corresponding to the first evidence of a bipolar signature in B_z. The onset of the plasmoid observation is the onset time of the event as observed at P2 and is thus used for our timing analysis, being the first observed sign of the event and having better timing resolution than the tailward streaming particles. The small fluctuations in B_z that precede the plasmoid are much smaller in magnitude and do not form an recognizable pattern so are not interpreted with any relation to the event's onset.

[26] If the flows are indeed due to reconnection, we expect the current sheet to resemble a slingshot-like standing Alfvén wave [*Øieroset et al.*, 2000]. We compared the change in flow velocity, ΔV_i, with the change in Alfvénic velocity, ΔV_A, during the time interval from when V_i starts turning tailward to its maximum velocity (0450:20–0452:45). $\Delta \mathbf{V_A} \sim \Delta \mathbf{B}/(N_i * \mu_o)^{1/2}$ where N_i is the ion density and **B** is the magnetic field. The stress balance at the peak velocity gives ratios: $|\Delta V_A|/|\Delta V_i| \sim 97\%$. These observations are consistent with Alfvénic acceleration, as expected from reconnection.

[27] We would like to point out that at 0447:10 there is a small Bz fluctuation, bipolar in nature, that correlates with an earthward anisotropy. Only 20 s later the anisotropy turns tailward as Bz turns southward. The timing of these plasma sheet activations would suggest they correspond with the precursory Pi2 activity at 0448:15 UT mentioned previously in our ground-based observations.

[28] We now turn out attention to P3, on the earthward side of the reconnecting plasma sheet (Figure 9). The observed onset time of the event at P3 is marked by a sharp increase in B_y on that probe at 0449:57 UT, interpreted as the passage of a field-aligned current pair, correlating with an increase in earthward anisotropy seen in Figure 9g. A second $+B_y$ pulse was observed at 0451 UT. Assuming that the motion of the plasma is to first order earthward/duskward, as measured by the plasma instrument, we interpret these field aligned current signatures as being due to field aligned current pairs of currents, moving earthward/dawnward over the probe. By 0452:30 UT B_y reached a level more positive than before the event, signifying the buildup of a unidirectional field aligned current into the ionosphere lobeward of P3. We interpret the latter as the signature of the buildup of the downward field aligned current of the substorm current wedge, consistent with the presence of P3 on the dawn side of the substorm meridian.

[29] It is evident from the angular anisotropy spectrogram in Figure 9f that the earthward anisotropy observed near the onset of the field aligned current signatures corresponds to an intensification of the 25–50 keV ions in the earthward direction, whereas prior to that time weak fluxes of mostly duskward ions (consistent with diamagnetic drift of ions) were observed. This indicates thinning of the cross-tail current sheet prior to the onset (the explosive growth phase). The following dawnward turn of the bulk velocity and coinciding magnetic field variations were interpreted as

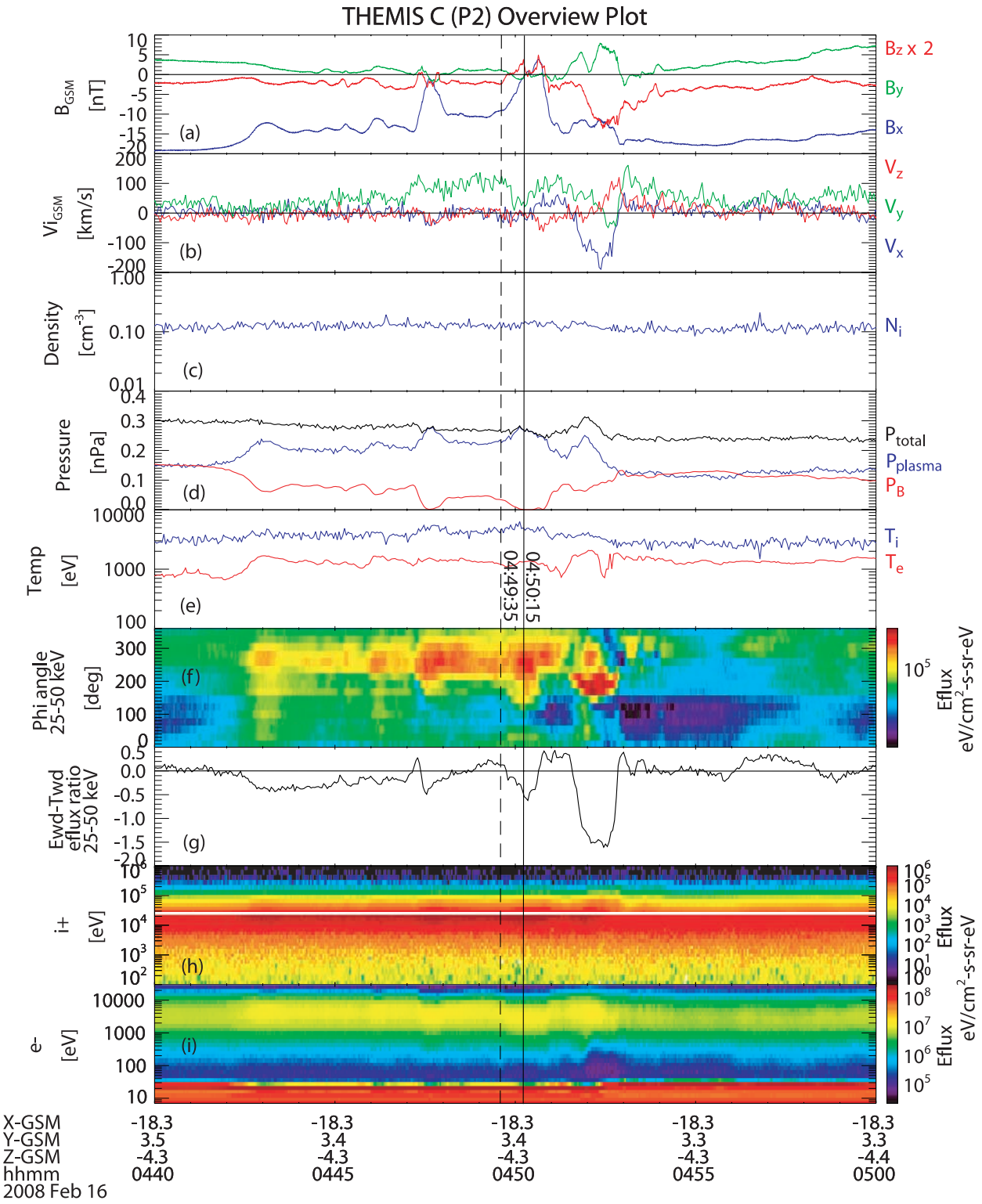

Figure 8. (a) The magnetic field as measured by P2 with Bz multiplied by 2 to enhance its features. (b–e) Particle data. (f) Energy flux of ions with energies between 25 and 50 keV. The *y* axis is the phi angle, where flux measured at 0° is a measure of earthward flowing particles and flux measured at 180° is a measure of tailward flowing particles. (g) The anisotropy of the particles, calculated as a ratio between energy fluxes (earthward-tailward divided by the average flux). (h and i) Ion and electron spectrograms, respectively. The observed onset time marked by the dashed vertical line at 0449:35 UT was chosen when P2 saw a jump in field-aligned ion particles seen in Figure 8f as well as a sudden increase in both Bx and Bz. Coincides with passage of an FTE in Figure 8a starting at the observed onset time. The solid vertical line at 0450:15 UT marks the time of the auroral brightening at SNKQ. In Figure 8b P2 sees a tailward flow.

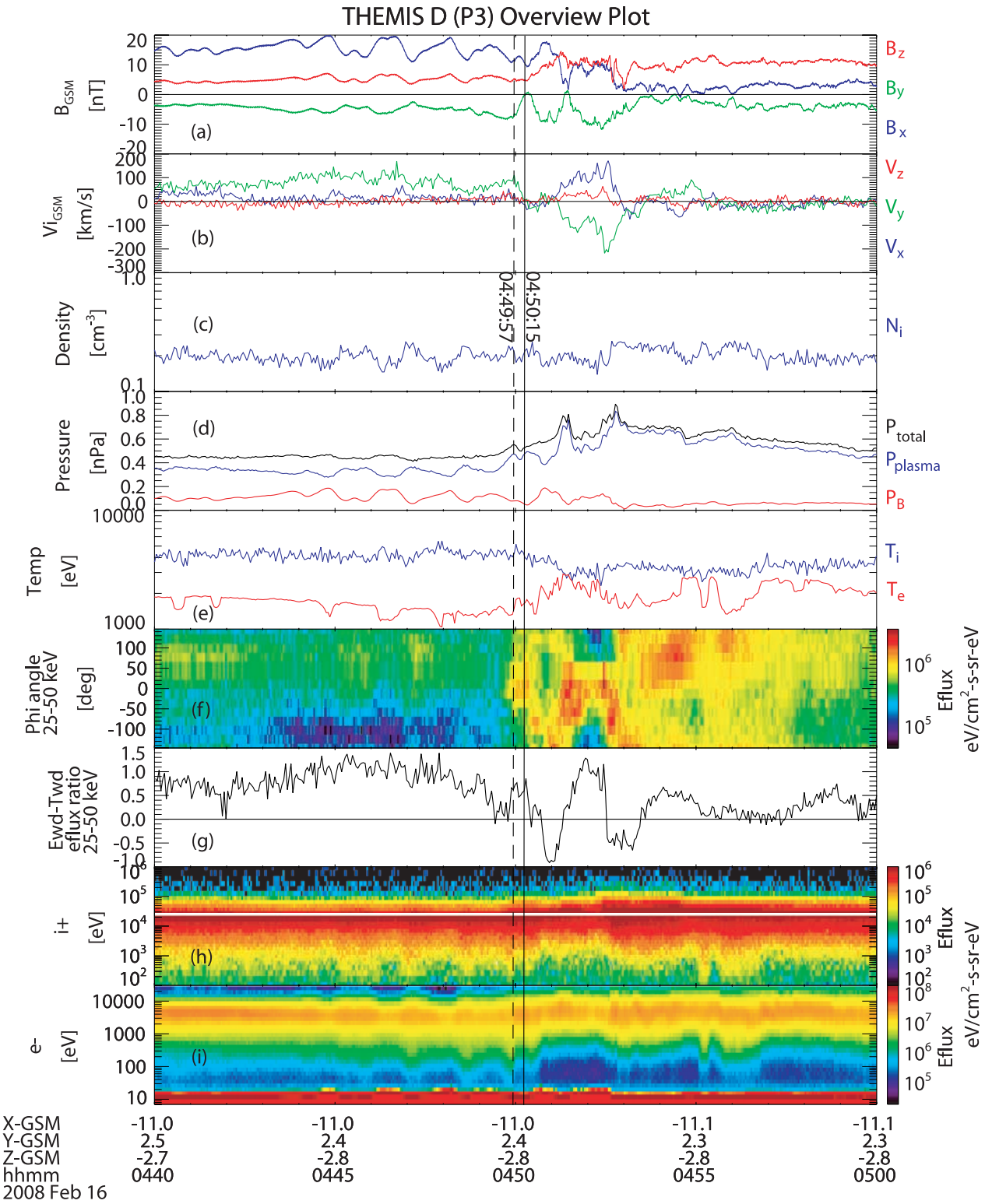

Figure 9. (a) The magnetic field as measured by P3. (b–e) Particle data. (f) Energy flux of particles with energies between 25 and 50 keV. The *y* axis is the phi angle, where flux measured at 0° is a measure of earthward flowing particles and flux measured at 180° is a measure of tailward flowing particles. (g) The anisotropy of the particles, calculated as a ratio between energy fluxes (earthward-tailward divided by the average flux). (h and i) Ion and electron spectrograms, respectively. The observed onset time marked by the vertical dashed line was chosen when P3 saw a sudden increase in By, correlating with a decrease in Vy, increase in Vx, decrease in Ti, increase in Te, and a definite jump in field-aligned ion particles seen in Figure 9f. The solid vertical line marks the auroral brightening seen at SNKQ. In Figure 9b P3 sees an earthward flow.

signatures of field-aligned current, generated by the reconnection outflow [*Sergeev et al.*, 1996b]. Thus the particle energization and dipolarization observed on P3 commenced with beam-like earthward ions and the passage of field aligned current pairs, ending with a relaxation of the cross tail current. The earthward anisotropy indicates that the heated plasma was moving earthward, contrary to the picture of outward motion of the current disruption discussed in previous papers [*Lui*, 1996].

[30] The following tailward anisotropy around 0452:30 is not surprising following a BBF such as this. After a BBF onset (or sometimes during BBFs) there are tailward flows observed, generally slower than the earthward ones preceding them, and can be attributed to two factors. The first is that slant crossings of a BBF structure can give you tailward flows at the edges of an earthward propelled flux tube, since the previously stationary plasma has to be pushed around and out of the way of the earthward flux tube of the BBF [*Sergeev et al.*, 1996b]. The second is recoil. As the BBF crashes in the near-Earth region, it cannot move through it because the Earth field is very strong. There are pressure gradients (magnetic, curvature) which develop and push the BBF back out. This recoil is often seen at the trailing edge of a BBF [*Chen and Wolf*, 1999]. Additionally, anisotropies can be due to beams which bounce back and forth in the plasma sheet.

[31] To determine the first arrival time of the signatures of reconnection at P3 we used the onset of the field aligned current pair and the inflection point of the dawnward flow, both at 0449:57 UT. These took place ~20 s after the energetic particle beams but ought to have propagated to P3 at the magnetosonic speed (or slower) and are thus better to use for the timing of reconnection onset. The field dipolarization (labeled current disruption, because the dipolarization started earlier than the earthward plasma flow) was observed 22 s after the first signatures of reconnection at 0450:19 UT. Both those times are transferred in Table 1.

[32] P4 saw an earthward flow and dipolarization as well. The observed duskward/dawnward fluctuations are indicative of plasma diversion. The measured dipolarization was sharper at P4 than P3 (see Figure 7), indicating that P4 was closer to the substorm meridian, however the response was delayed. We interpret the delay as being due to the earthward separation between P3 and P4 (see Figure 1). To obtain the best timing results, we take the earliest indication of dipolarization. Mapping to the ground is favorable and we expect that both probes are within the substorm current wedge, very close to the substorm meridian. This expectation is supplemented by the model in Figure 3.

4. Relative Timing

[33] Using the observed onset times we determined at P2 and P3 and making the assumption that the information travels at a constant speed both tailward and earthward of the acceleration site, we calculate the location and onset times of potential reconnection sites (solid red line in Figure 10) and times (solid blue line in Figure 10) as a function of the propagation speed. Assuming that information is traveling at magnetosonic speeds, we can measure what those speeds are at P2 and P3 to place limits site location and onset times. The maximum magnetosonic speed is $V_{MS} \sim (V_A^2 + V_{TH}^2)^{1/2}$ where V_{TH} is the particle thermal velocity. Using local measurements of density, temperature and field magnitude we obtain a magnetosonic speed of ~600 km/s at P3 and ~730 km/s at P2 (see vertical lines V_U and V_L respectively in Figure 10). On the basis of those, we expect the reconnection site to lie within 15.6 and 15.9 R_E downtail, and the reconnection onset time to be between 0449:07 UT and 0449:14 UT. This time is also transferred into Table 1 and is used to compute a delay time relative to reconnection onset in Table 1 as well as in Figure 1. Since the reconnection time corresponds to a range of times, we use the middle time, 0449:11 UT, as the start time. Since V_{TH} goes as $Ti^{1/2}$ and V_A as $1/Ni^{1/2}$ (assuming constant $|B|$) where Ti is the ion temperature and Ni the density, as a first-order approximation we see that V_{MS} only varies as 3.4 km/s. This estimation indicates that our timing method, utilizing a constant velocity in the vicinity of the neutral sheet, is good in the first-order approximation.

[34] It is evident from Table 1 that reconnection preceded the onset of auroral intensification by 64 s, and the onset of dipolarization at P3 by 68 s. This suggests that reconnection onset was likely the process by which both of those phenomena were initiated, and that current disruption could not have been causally responsible for auroral brightening. Auroral Pi2 pulsations were seen 89 s after reconnection onset, which is consistent with the expected delay time for Alfvén waves to travel from the equatorial plasma sheet at 16 R_E to the ionosphere. The poleward expansion of the aurora was observed to start 91 s after reconnection onset and only 23 s after the first observed signatures of current disruption. This suggests that the poleward expansion of the aurora is not initiated by dipolarization at the inner edge of the plasma sheet, but rather as a result of topological reconfigurations of the plasma sheet as a result of plasma sheet field line reconnection. The midlatitude Pi2s were seen 71 s after near-Earth dipolarization and 139 s after reconnection onset. The midlatitude Pi2 generation is consistent with the establishment of a large-scale substorm current wedge. Fast flow generated currents [*Kepko et al.*, 2004], emanating from the reconnection site may be also able to establish a field aligned current system of the same sense as the substorm current wedge, and be responsible for the early portion of the midlatitude Pi2 activity. Given an Alfvén propagation time of 90 s, needed to establish the initial substorm current wedge system via Alfvén waves, this initial time delay is consistent with bursty bulk flows emanating from the reconnection site, and launching an

Table 1. Timing of Events

Event	Observed Timing (UT)	Inferred Delay (Seconds Since 0449:11 UT)
Reconnection (timing analysis)	0449:07–0449:14	TRx = 0
Reconnection effects at P2	0449:35	24
Reconnection effects at P3	0449:57	46
Auroral intensification (integrated intensity)	0450:15	TAI = 64
Dipolarization onset (at P3)	0450:19	TCD = 68
Auroral Pi2 (SNKQ)	0450:40	89
Auroral poleward expansion (SNKQ ASI)	0450:42	91
Midlatitude Pi2 (PINE)	0451:30	139
AE rise	0451:35	144

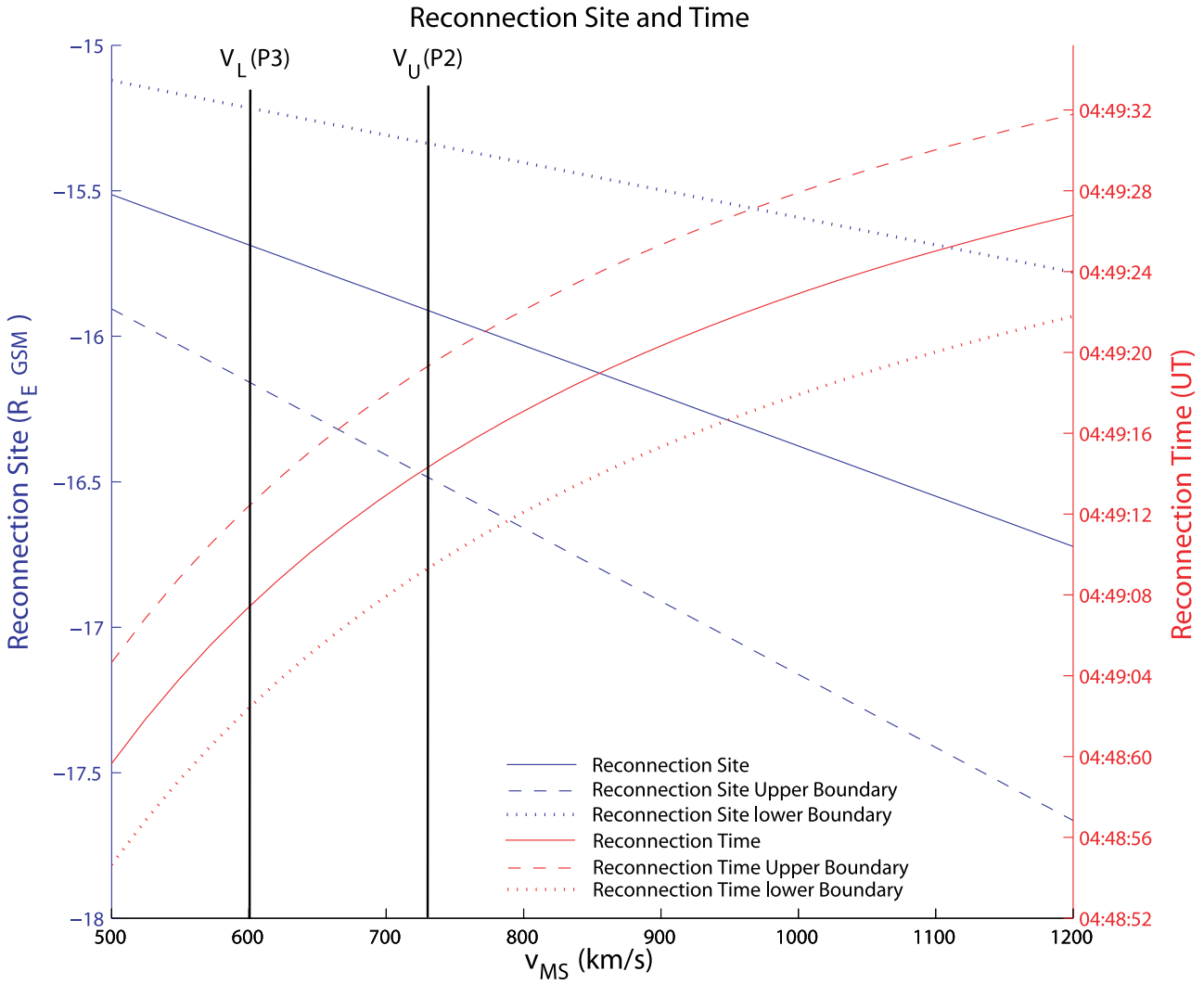

Figure 10. Graphical representation of possible reconnection sites and onset times. V_L (604 km/s) and V_U (730 km/s) are the calculated lower and upper limit of maximum travel speeds expected on the basis of the observed magnetosonic speeds at P2 and P3. The dashed lines (upper and lower boundary) are a measure of the solution uncertainty assuming our choices of onset times at P2 and P3 are off by ±5 s.

initial field aligned current system prior to the establishment of a global substorm current wedge through the interaction with the inner magnetosphere. It is noteworthy that the global substorm electrojet current system (based on AE_{TH}) gets established only seconds after the establishment of global Pi2 waves and more than 40 s after the start of poleward auroral expansion.

5. Discussion and Conclusions

[35] With the unprecedented spacecraft alignments and time resolution afforded by the THEMIS constellation and ground-based observatories, we have performed a timing analysis of the sequence of events that leads to substorm onset at 0450 UT on 16 February 2008. Specifically it is possible to differentiate and delineate different traditional substorm onset observables and determine the causal relationship between underlying physical processes responsible for them. The results presented regarding this substorm are consistent with the analysis of the substorm on 0450 UT of 26 February 2008 described by *Angelopoulos et al.* [2008]. Specifically we have shown that expansion phase onset in the tail at ~15.8 R_E precedes any substorm onset definition the reader chooses for identification, and results in the sequence of near-Earth tail and ionospheric events which make up the magnetospheric substorm.

[36] Additionally, we have noted that this substorm did not start as an isolated activation in the plasma sheet or in the ionosphere. Rather, the substorm onset took place after a series of auroral and plasma sheet activations, at least two of which are related to intensifications of a preexisting high-latitude auroral arc. Despite the high-latitude arc's temporal and spatial proximity to the substorm arc it appears that it did not initiate onset. Our results indicate that the plasma sheet may be active prior to substorm onset but reconnection does not always reach a critical enough stage to have global magnetospheric consequences. An open question therefore is what physical process controls onset of reconnection and what determines its quenching or eventual

growth on a global scale, at sites which have such close temporal and spatial proximity in the magnetotail.

[37] **Acknowledgments.** We acknowledge NASA contract NAS5-02099 for use of data from the THEMIS Mission and the German Ministry for Economy and Technology and the German Center for Aviation and Space (DLR) under contract 50 OC 0302 for FGM data. The orbit images were obtained from NASA through the SSCWeb 3D orbital viewer program TIPSOD. CARISMA is operated by the University of Alberta and funded by the Canadian Space Agency. The Canadian Magnetic Observatory System (CANMOS) network, maintained and operated by the Geological Survey of Canada, also provided data used in this study. We would like to acknowledge Jiang Liu for producing the timing code and the UCLA IGPP programmers for their help and advice.

[38] Wolfgang Baumjohann thanks Victor Sergeev and another reviewer for their assistance in evaluating this paper.

References

Akasofu, S.-I. (1964), The development of the auroral substorm, *Planet. Space Sci.*, *12*, 273–282, doi:10.1016/0032-0633(64)90151-5.

Angelopoulos, V. (2008), The THEMIS mission, *Space Sci. Rev.*, doi:10.1007/s11214-008-9336-1, in press.

Angelopoulos, V., et al. (1997), Magnetotail flow bursts: Association to global magnetospheric circulation, relationship to ionospheric activity and direct evidence for localization, *Geophys. Res. Lett.*, *24*(18), 2271–2274, doi:10.1029/97GL02355.

Angelopoulos, V., et al. (2008), First Results from the THEMIS Mission, *Space Sci. Rev.*, doi:10.1007/s11214-008-9378-4, in press.

Auster, H. U., et al. (2008), The THEMIS fluxgate magnetometer, *Space Sci. Rev.*, doi:10.1007/s11214-008-9365-9, in press.

Baker, D., T. Pulkkinen, V. Angelopoulos, W. Baumjohann, and R. McPherron (1996), Neutral line model of substorms: Past results and present view, *J. Geophys. Res.*, *101*(A6), 12,975–13,010, doi:10.1029/95JA03753.

Baumjohann, W., et al. (2007), Dynamics of thin current sheets: Cluster observations, *Ann. Geophys.*, *25*, 1365–1389.

Chen, C., and R. Wolf (1999), Theory of thin-filament motion in Earth's magnetotail and its application to bursty bulk flows, *J. Geophys. Res.*, *104*(A7), 14,613–14,626, doi:10.1029/1999JA900005.

Harris, S. E., et al. (2008), THEMIS ground-based observatory system design, *Space Sci. Rev.*, *141*, 213–233, doi:10.1007/s11214-007-9294-z.

Horning, B. L., R. L. McPherron, and D. D. Jackson (1974), Application of linear inverse theory to a line current model of substorm current systems, *J. Geophys. Res.*, *79*(34), 5202–5210, doi:10.1029/JA079i034p05202.

Ieda, A., S. Machida, T. Mukai, Y. Saito, T. Yamamoto, A. Nishida, T. Terasawa, and S. Kokubun (1998), Statistical analysis of the plasmoid evolution with Geotail observations, *J. Geophys. Res.*, *103*, 4453–4466, doi:10.1029/97JA03240.

Kepko, L., M. G. Kivelson, and R. L. McPherron (2004), Relative timing of substorm onset phenomena, *J. Geophys. Res.*, *109*, A04203, doi:10.1029/2003JA010285.

Liou, K., C.-I. Meng, A. T. Y. Lui, P. T. Newell, and S. Wing (2002), Magnetic dipolarization with substorm expansion onset, *J. Geophys. Res.*, *107*(A7), 1131, doi:10.1029/2001JA000179.

Lui, A. (1996), Current disruption in the Earth's magnetosphere: Observations and models, *J. Geophys. Res.*, *101*(A6), 13,067–13,088, doi:10.1029/96JA00079.

Lui, A. T. Y., et al. (2007), Prelude to THEMIS tail conjunction study, *Ann. Geophys.*, *25*, 1001–1009.

Mayaud, P. N. (1980), *Derivation, Meaning and Use of Geomagnetic Indices*, *Geophys. Monogr. Ser.*, vol. 22, AGU, Washington, D. C.

McFadden, J. P., C. W. Carlson, D. Larson, V. Angelopoulos, M. Ludlam, R. Abiad, and B. Elliot (2008), The THEMIS ESA plasma instrument and in-flight calibration, *Space Sci. Rev.*, in press.

Mende, S. B., V. Angelopoulos, H. U. Frey, S. Harris, E. Donovan, B. Jackel, M. Syrjaesuo, C. T. Russell, and I. Mann (2007), Determination of substorm onset timing and location using the THEMIS ground based observatories, *Geophys. Res. Lett.*, *34*, L17108, doi:10.1029/2007GL030850.

Mende, S. B., S. E. Harris, H. U. Frey, V. Angelopoulos, C. T. Russell, E. Donovan, B. Jackel, M. Greffen, and L. M. Peticolas (2008), The THEMIS array of ground-based observatories for the study of auroral substorms, *Space Sci. Rev.*, doi:10.1007/s11214-008-9380-x, in press.

Milling, D. K., I. J. Rae, I. R. Mann, K. R. Murphy, A. Kale, C. T. Russell, V. Angelopoulos, and S. Mende (2008), Ionospheric localisation and expansion of long-period Pi1 pulsations at substorm onset, *Geophys. Res. Lett.*, *35*, L17S20, doi:10.1029/2008GL033672.

Murphy, K. R., I. J. Rae, I. R. Mann, D. K. Milling, C. E. J. Watt, L. Ozeke, H. U. Frey, V. Angelopoulos, and C. T. Russell (2008), Wavelet-based ULF wave diagnosis of substorm expansion phase onset, *J. Geophys. Res.*, doi:10.1029/2008JA013548, in press.

Ohtani, S., and S. Kokubun (1991), Magnetic properties of the high-latitude tail boundary: Draping of magnetosheath field lines and tail-aligned current, *J. Geophys. Res.*, *96*(A6), 9521–9530, doi:10.1029/91JA00570.

Øieroset, M., T. D. Phan, R. P. Lin, and B. U. O. Sonnerup (2000), Walén and variance analyses of high-speed flows observed by Wind in the midtail plasma sheet: Evidence for reconnection, *J. Geophys. Res.*, *105*, 25,247–25,264, doi:10.1029/2000JA900075.

Rae, J., et al. (2009), Timing and localization of ionospheric signatures associated with substorm expansion phase onset, *J. Geophys. Res.*, *114*, A00C09, doi:10.1029/2008JA013559.

Rostoker, G., S.-I. Akasofu, J. Foster, R. Greenwald, Y. Kamide, K. Kawasaki, A. Lui, R. McPherron, and C. Russell (1980), Magnetospheric substorms: Definition and signatures, *J. Geophys. Res.*, *85*(A4), 1663–1668, doi:10.1029/JA085iA04p01663.

Russell, C. T., P. J. Chi, D. J. Dearborn, Y. S. Ge, B. Kuo-Tiong, J. D. Means, D. R. Pierce, K. M. Rowe, and R. C. Snare (2009), THEMIS ground-based magnetometers, *Space Sci. Rev.*, doi:10.1007/s11214-008-9337-0, in press.

Sergeev, V., V. Angelopoulos, D. Mitchell, and C. Russell (1995), In situ observations of magnetotail reconnection prior to the onset of a small substorm, *J. Geophys. Res.*, *100*(A10), 19,121–19,133, doi:10.1029/95JA01471.

Sergeev, V. A., L. I. Vagina, R. D. Elphinstone, J. S. Murphree, D. J. Hearn, L. L. Cogger, and M. L. Johnson (1996a), Comparison of UV optical signatures with the substorm current wedge as predicted by an inversion algorithm, *J. Geophys. Res.*, *101*(A2), 2615–2627, doi:10.1029/95JA00537.

Sergeev, V., V. Angelopoulos, J. Gosling, C. Cattell, and C. Russell (1996b), Detection of localized, plasma-depleted flux tubes or bubbles in the midtail plasma sheet, *J. Geophys. Res.*, *101*(A5), 10,817–10,826, doi:10.1029/96JA00460.

Starkov, G. V., M. I. Pudovkin, and T. A. Kornilova (2006), Auroral fading structure before breakup: A review, *Geomagn. Aeron.*, *46*(1), 1–14.

Tsyganenko, N. (1995), Modeling the Earth's magnetospheric magnetic field confined within a realistic magnetopause, *J. Geophys. Res.*, *100*(A4), 5599–5612, doi:10.1029/94JA03193.

Zesta, E., L. Lyons, C.-P. Wang, E. Donovan, H. Frey, and T. Nagai (2006), Auroral poleward boundary intensifications (PBIs): Their two-dimensional structure and associated dynamics in the plasma sheet, *J. Geophys. Res.*, *111*, A05201, doi:10.1029/2004JA010640.

V. Angelopoulos, C. Gabrielse, A. Runov, and C. T. Russell, IGPP, ESS, University of California, P.O. Box 951567, Los Angeles, CA 90095, USA. (cgabrielse@ucla.edu)

S. Apatenkov, University of St. Petersburg, St. Petersburg, 198504, Russia.

H. U. Frey, D. E. Larson, J. McFadden, and S. Mende, Space Sciences Laboratory, University of California, Berkeley, CA 94720, USA.

K.-H. Glassmeier, Technische Universität Braunschweig, D-38106 Braunschweig, Germany.

K. R. Murphy and I. J. Rae, Department of Physics, University of Alberta, Edmonton, AB T6G 2G7, Canada.